

Methane Activation on Single-Atom Ir-doped Metal Nanoparticles from First-principles

Yugang Ren¹, Xiaojing Liu¹, Zhaojun Zhang², Xiangjian Shen*¹

Table of content

| | |
|--|---|
| SI-1: Transition state information on the pure metal surface | 2 |
| SI-2: Information on the transition state of the alloy surface | 3 |
| SI-3: Transition state Bader-charge analysis | 3 |
| SI-4: Surface energy of each alloy crystal plane (J/m ²) | 3 |
| SI-5: Proportions of (100), (110) and (111) surfaces of pure metal nanoparticles under two different given pressures at T=500 K | 4 |
| SI-6: Proportions of (100), (110) and (111) surfaces of alloy metal nanoparticles under two different given pressures at T=500 K | 4 |
| SI-7: Proportions of (100), (110) and (111) surfaces of alloy metal nanoparticles under different temperatures at P=1bar | 5 |
| SI-8: The pure metal activity (S ⁻¹) | 5 |
| SI-9: The alloy activity (S ⁻¹) | 5 |
| SI-10: The dissociation barrier of methane and adsorption energy of methyl on Ni(111) surface with and without the van der Waals correction | 5 |
| SI-11: Wulff structures of pure-metals at different pressures | 6 |
| SI-12: Wulff structures of pure-metals at different temperatures | 7 |
| SI-13: Transition states of methane activation on different pure metal surfaces including (100), (110) and (111) surfaces. | 8 |
| SI-14: Transition states of methane activation on different alloy metal surfaces including (100), (110) and (111) surfaces. | 8 |
| SI-15: Wulff structures of Ir@M alloy at different pressures | 9 |
| SI-16: Wulff structures of Ir@M alloy at different temperatures | 9 |

Table S1: Transition state information on the pure metal surface.

| | | rigid | | | | relaxed | | | |
|-----------|------------|-----------------|-----------------|-----------------|---------------|-----------------|-----------------|-----------------|---------------|
| | | d_{MC} (Å) | R_{CH} (Å) | θ (°) | E_b (eV) | d_{MC} (Å) | R_{CH} (Å) | θ (°) | E_b (eV) |
| Co | 100 | 2.093 | 1.613 | 132 | 0.851 | 2.067 | 1.611 | 132 | 0.791 |
| | 110 | 2.099 | 1.662 | 125 | 0.999 | 2.058 | 1.681 | 128 | 0.894 |
| | 111 | 2.147 | 1.614 | 128 | 1.082 | 2.111 | 1.732 | 125 | 0.993 |
| Rh | 100 | 2.223 | 1.57 | 130 | 0.674 | 2.205 | 1.556 | 130 | 0.596 |
| | 110 | 2.205 | 1.625 | 127 | 0.716 | 2.203 | 1.598 | 131 | 0.653 |
| | 111 | 2.147 | 1.614 | 128 | 1.082 | 2.111 | 1.732 | 125 | 0.993 |
| Ir | 100 | 2.283 | 1.452 | 133 | 0.555 | 2.283 | 1.441 | 133 | 0.463 |
| | 110 | 2.263 | 1.568 | 127 | 0.477 | 2.25 | 1.525 | 127 | 0.374 |
| | 111 | 2.297 | 1.581 | 129 | 0.892 | 2.259 | 1.49 | 132 | 0.716 |
| Ni | 100 | 2.065 | 1.629 | 126 | 0.934 | 2.025 | 1.643 | 127 | 0.807 |
| | 110 | 2.036 | 1.642 | 126 | 0.761 | 2.022 | 1.658 | 129 | 0.717 |
| | 111 | 2.108 | 1.696 | 127 | 1.043 | 2.057 | 1.547 | 136 | 0.886 |
| Pd | 100 | 2.174 | 1.634 | 132 | 0.740 | 2.157 | 1.608 | 132 | 0.644 |
| | 110 | 2.170 | 1.587 | 134 | 0.722 | 2.157 | 1.638 | 132 | 0.692 |
| | 111 | 2.204 | 1.687 | 131 | 0.873 | 2.180 | 1.657 | 130 | 0.819 |
| Pt | 100 | 2.267 | 1.449 | 135 | 0.604 | 2.231 | 1.414 | 135 | 0.447 |
| | 110 | 2.240 | 1.477 | 132 | 0.383 | 2.234 | 1.459 | 132 | 0.346 |
| | 111 | 2.257 | 1.532 | 131 | 0.845 | 2.224 | 1.524 | 129 | 0.734 |

Table S2: Information on the transition state of the alloy surface.

| relaxed | | | | rigid | | | | | | |
|--------------|---------------|-----------------|-----------------|-----------------|---------------|-----------------|-----------------|-----------------|---------------------|-------|
| | E_b (eV) | R_{CH} (Å) | d_{MC} (Å) | θ (°) | E_b (eV) | R_{CH} (Å) | d_{MC} (Å) | θ (°) | $d_{Ir-Ir'}$ (Å) | |
| Ir@Rh | 100 | 0.506 | 1.420 | 2.277 | 132 | 0.613 | 1.43 | 2.30 | 132 | 0.131 |
| | 110 | 0.437 | 1.474 | 2.250 | 119 | 0.541 | 1.52 | 2.26 | 124 | 0.108 |
| | 111 | 0.697 | 1.483 | 2.621 | 129 | 0.833 | 1.52 | 2.30 | 130 | 0.200 |
| Ir@Ni | 100 | 0.488 | 1.447 | 2.268 | 133 | 0.569 | 1.45 | 2.30 | 133 | 0.130 |
| | 110 | 0.481 | 1.482 | 2.228 | 131 | 0.578 | 1.52 | 2.24 | 136 | 0.123 |
| | 111 | 0.644 | 1.507 | 2.258 | 128 | 0.811 | 1.52 | 2.32 | 133 | 0.198 |
| Ir@Pd | 100 | 0.331 | 1.360 | 2.275 | 133 | 0.529 | 1.47 | 2.32 | 132 | 0.192 |
| | 110 | 0.100 | 1.450 | 2.229 | 122 | 0.240 | 1.49 | 2.24 | 125 | 0.098 |
| | 111 | 0.290 | 1.417 | 2.263 | 128 | 0.539 | 1.51 | 2.28 | 131 | 0.234 |

| | | | | | | | | | | |
|--------------|------------|-------|-------|-------|-----|-------|------|------|-----|-------|
| | 100 | 0.237 | 1.392 | 2.259 | 133 | 0.401 | 1.40 | 2.30 | 133 | 0.185 |
| Ir@Pt | 110 | 0.014 | 1.430 | 2.233 | 119 | 0.100 | 1.51 | 2.24 | 121 | 0.089 |
| | 111 | 0.382 | 1.485 | 2.229 | 128 | 0.633 | 1.52 | 2.28 | 131 | 0.271 |
| | 100 | 0.433 | 1.458 | 2.26 | 131 | 0.539 | 1.47 | 2.30 | 133 | 0.174 |
| Ir@Cu | 110 | 0.335 | 1.461 | 2.212 | 137 | 0.402 | 1.50 | 2.23 | 133 | 0.133 |
| | 111 | 0.471 | 1.490 | 2.279 | 129 | 0.626 | 1.52 | 2.32 | 131 | 0.214 |
| | 100 | 0.302 | 1.420 | 2.525 | 130 | 0.502 | 1.44 | 2.29 | 131 | 0.164 |
| Ir@Ag | 110 | 0.114 | 1.401 | 2.222 | 134 | 0.176 | 1.43 | 2.24 | 133 | 0.110 |
| | 111 | 0.301 | 1.439 | 2.273 | 129 | 0.498 | 1.49 | 2.31 | 131 | 0.240 |

Table S3: Transition state Bader-charge analysis(e).

| | | relaxed | | |
|--------------|------------|-----------------|---------|--------|
| | | CH ₃ | Ir | H |
| Ir@Rh | 100 | -0.0554 | 0.0195 | 0.0602 |
| | 110 | -0.0504 | -0.0297 | 0.0712 |
| | 111 | -0.0255 | -0.101 | 0.0757 |
| Ir@Ni | 100 | -0.0568 | -0.247 | 0.0520 |
| | 110 | -0.0578 | -0.219 | 0.0500 |
| | 111 | -0.0568 | -0.284 | 0.0580 |
| Ir@Pd | 100 | -0.0319 | 0.0607 | 0.0730 |
| | 110 | -0.0166 | 0.0462 | 0.0807 |
| | 111 | -0.0185 | 0.00144 | 0.0885 |
| Ir@Pt | 100 | -0.0115 | 0.165 | 0.0889 |
| | 110 | -0.0135 | 0.182 | 0.0797 |
| | 111 | 0.0258 | 0.135 | 0.107 |
| Ir@Cu | 100 | -0.0345 | -0.382 | 0.0272 |
| | 110 | -0.0653 | -0.313 | 0.0418 |
| | 111 | -0.0551 | -0.447 | 0.0509 |
| Ir@Ag | 100 | -0.0340 | -0.230 | 0.0398 |
| | 110 | -0.0363 | -0.216 | 0.0427 |
| | 111 | -0.0722 | -0.249 | 0.0548 |

Table S4: Surface energy of alloy crystal plane (J/m²).

| | | E _M ^{clean} | 300K | 500K | 700K |
|--------------|------------|---------------------------------|----------------------|----------------------|----------------------|
| | | | E _{surface} | E _{surface} | E _{surface} |
| Ir@Rh | 100 | 2.434 | 2.463 | 2.534 | 2.61 |
| | 110 | 2.457 | 2.472 | 2.522 | 2.576 |
| | 111 | 2.059 | 2.115 | 2.196 | 2.285 |
| Ir@Ni | 100 | 1.934 | 1.966 | 2.047 | 2.136 |
| | 110 | 2.090 | 2.110 | 2.168 | 2.231 |

| | | | | | |
|--------------|------------|-------|-------|-------|-------|
| | 111 | 1.537 | 1.598 | 1.692 | 1.795 |
| | 100 | 1.682 | 1.694 | 1.761 | 1.834 |
| Ir@Pd | 110 | 1.702 | 1.701 | 1.749 | 1.800 |
| | 111 | 1.497 | 1.521 | 1.598 | 1.682 |
| Ir@Pt | 100 | 1.937 | 1.932 | 1.998 | 2.070 |
| | 110 | 1.979 | 1.958 | 2.005 | 2.055 |
| | 111 | 1.588 | 1.603 | 1.679 | 1.761 |

Table S5: Proportions of (100), (110) and (111) surfaces of pure metal nanoparticles under two different given pressures at T=500 K

| | | 100 | 110 | 111 |
|-----------|----------------|------------|------------|------------|
| Rh | P=1bar | 21% | 11% | 68% |
| | P=10bar | 21% | 10% | 69% |
| Ir | P=1bar | 20% | 0% | 80% |
| | P=10bar | 19% | 0% | 81% |
| Ni | P=1bar | 23% | 0% | 77% |
| | P=10bar | 22.4% | 0% | 77.6% |
| Pd | P=1bar | 26% | 17% | 57% |
| | P=10bar | 26% | 16% | 58% |
| Pt | P=1bar | 22% | 5% | 73% |
| | P=10bar | 22% | 4% | 74% |

Table S6: Proportions of (100), (110) and (111) surfaces of alloy metal nanoparticles under two different given pressures at T=500 K.

| | | 100 | 110 | 111 |
|--------------|----------------|------------|------------|------------|
| Ir@Rh | P=1bar | 22% | 15% | 63% |
| | P=10bar | 22% | 14% | 64% |
| Ir@Ni | P=1bar | 18% | 0% | 82% |
| | P=10bar | 17% | 0% | 83% |
| Ir@Pd | P=1bar | 24% | 25% | 51% |
| | P=10bar | 24% | 25% | 51% |

| | | | | |
|--------------|----------------|-------|------|-------|
| Ir@Pt | P=1bar | 19.4% | 5.6% | 75% |
| | P=10bar | 19.2% | 4.4% | 76.4% |

Table S7: Proportions of (100), (110) and (111) surfaces of alloy metal nanoparticles under different temperatures at P=1bar.

| | 300K | | | 500K | | | 700K | | |
|--------------|------|-----|-----|-------|------|-----|------|-----|-----|
| | 100 | 110 | 111 | 100 | 110 | 111 | 100 | 110 | 111 |
| Ir@Rh | 22% | 10% | 68% | 22% | 15% | 63% | 22% | 19% | 59% |
| Ir@Ni | 16% | 0% | 84% | 18% | 0% | 82% | 19% | 0% | 81% |
| Ir@Pd | 24% | 20% | 56% | 24% | 25% | 51% | 24% | 31% | 45% |
| Ir@Pt | 18% | 0% | 82% | 19.4% | 5.6% | 75% | 20% | 11% | 69% |

Table S8: The pure metal activity(S⁻¹).

| Rh | Ir | Ni | Pd | Pt |
|--------|--------|--------|--------|--------|
| 20.168 | 19.330 | 14.405 | 17.551 | 19.759 |

Table S9: The alloy activity(S⁻¹).

| | 300K | 500K | 700K |
|--------------|--------|--------|--------|
| Ir@Rh | 15.745 | 20.741 | 23.840 |
| Ir@Ni | 12.862 | 16.902 | 19.443 |
| Ir@Pd | 19.049 | 21.476 | 23.533 |
| Ir@Pt | 18.242 | 23.785 | 25.819 |

Table S10: The dissociation barrier of methane and adsorption energy of methyl on Ni(111) surface with and without the van der Waals correction.

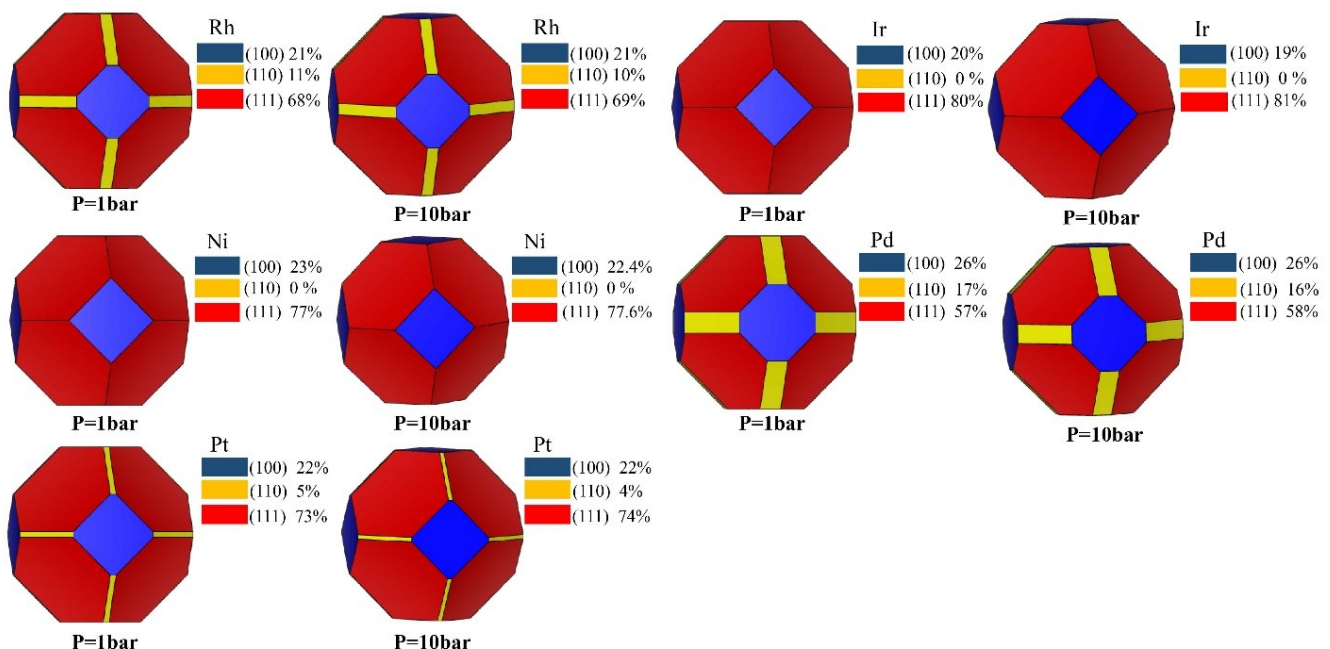
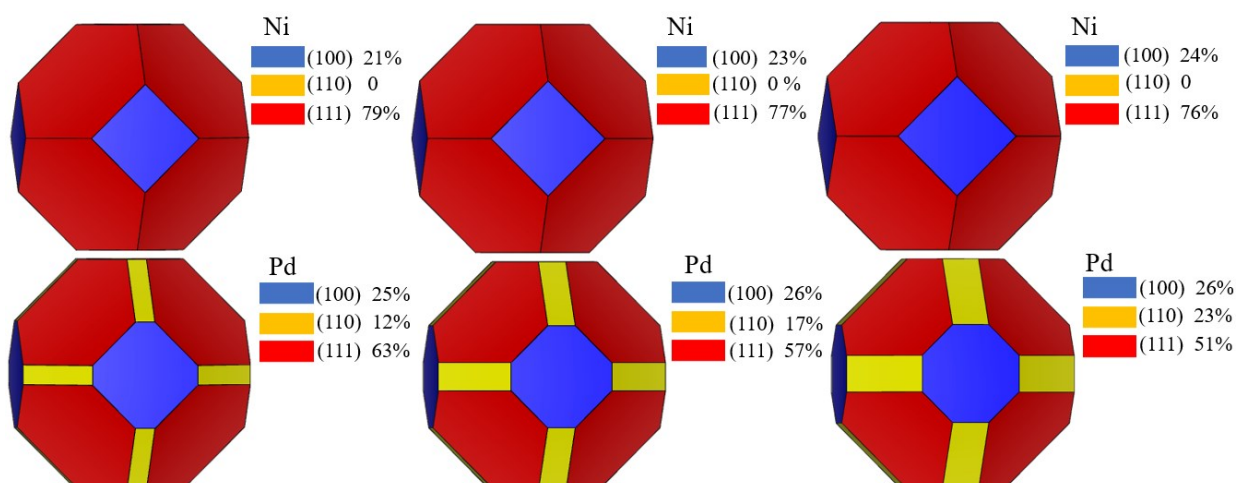
| | Uncorrected | Van der Waals correction |
|---|-------------|-----------------------------|
| Dissociation barrier(E_b/eV) | 0.886 | 0.575 |

Adsorption energy(E_{ads} /eV)

-2.344

-2.650

* Using DFT calculations (DFT-D3), the energy barrier and the adsorption energy of methyl with and without van der Waals correction are shown in Table S10. With the van der Waals correction, it is found that the energy barrier is decreased from 0.886 eV to 0.575 eV. Compared with the previous works, it is found that the adsorption energy of methyl on Ni(111) surface is closed to those previous results, e.g., -2.24 eV obtained by Lai et al. [1], -1.97 eV obtained by Wang et al. [2], -1.98 eV obtained by Zhu et al. [3], -2.60 eV obtained by Upton et al. [4] and -1.86 eV obtained by Wonchoba and Truhlar[5]. The van der Waals correction strengthens the adsorption energy of methyl on the Ni(111) surface.

FigureS1: Wulff structures of Ni, Pd, Pt, Rh and Ir metals at different pressures.**FigureS2:** Wulff structures of Ni, Pd, Pt, Rh and Ir metals at different temperatures.

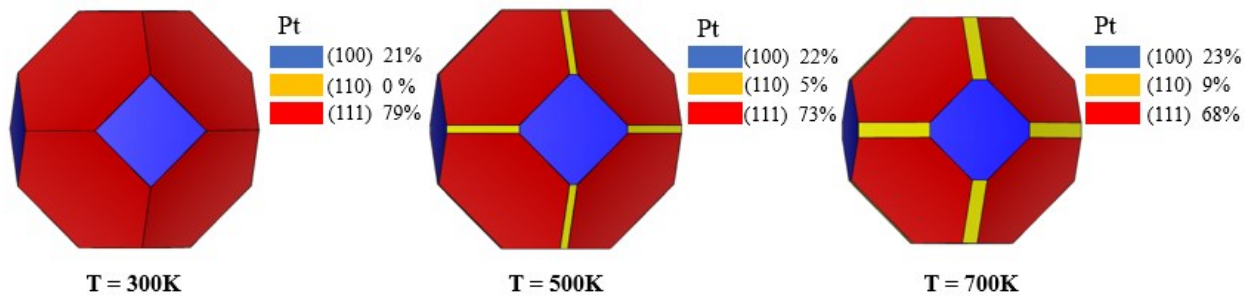


Figure S3: Transition states of methane activation on different pure metal surfaces including (100), (110) and (111) surfaces.

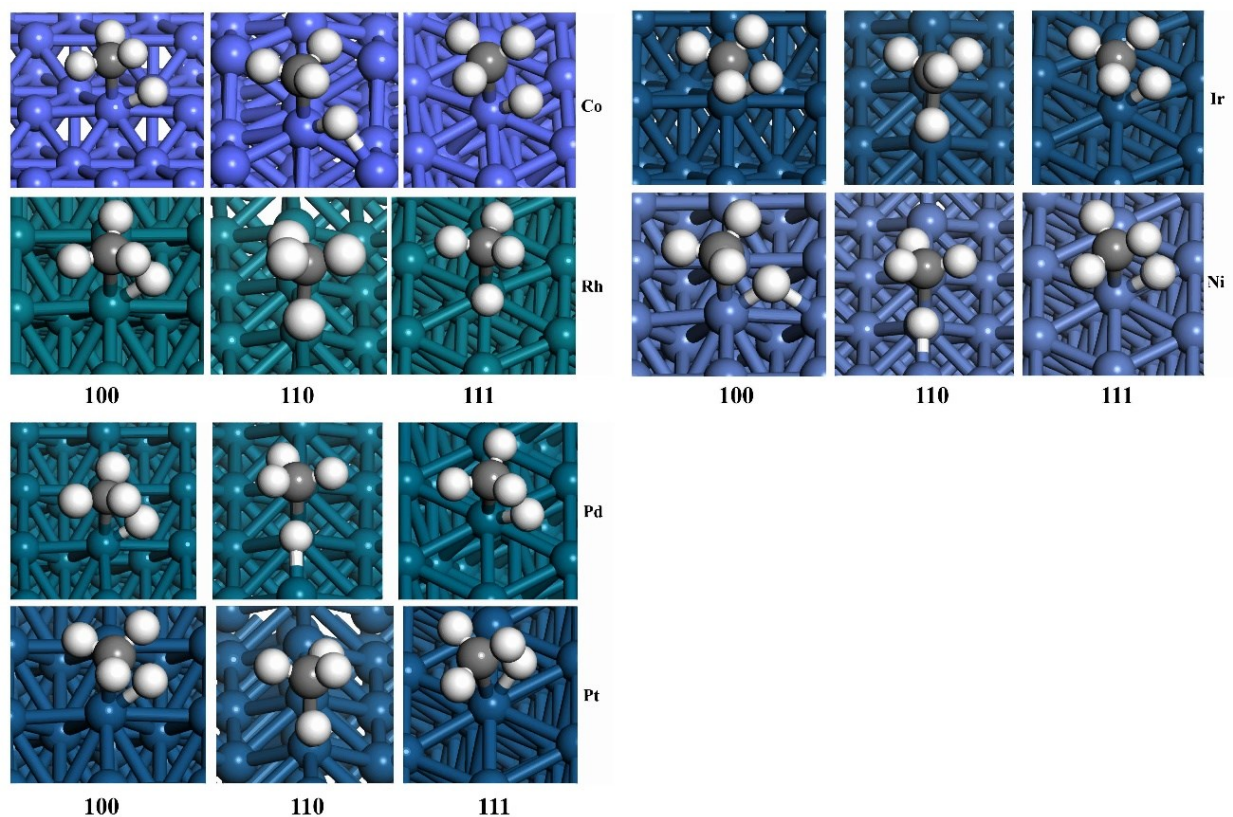
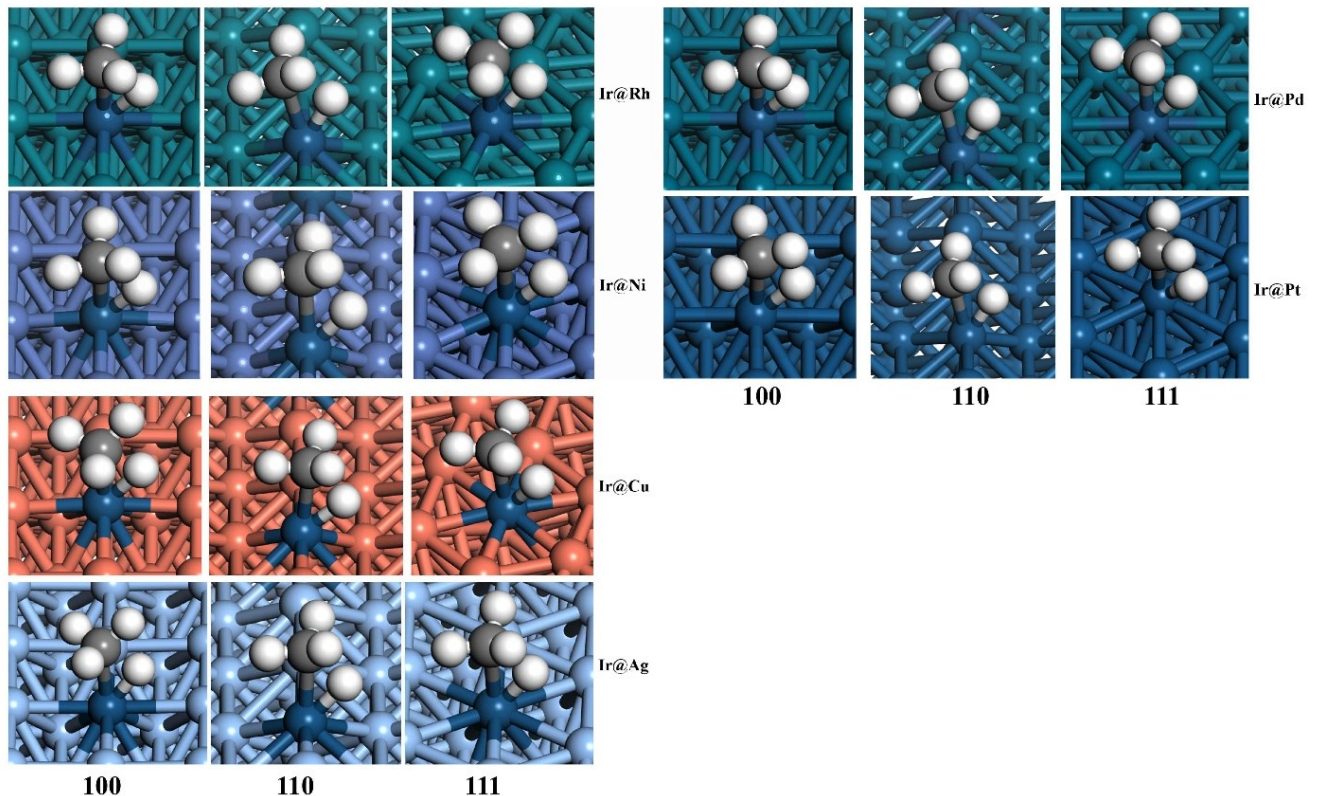
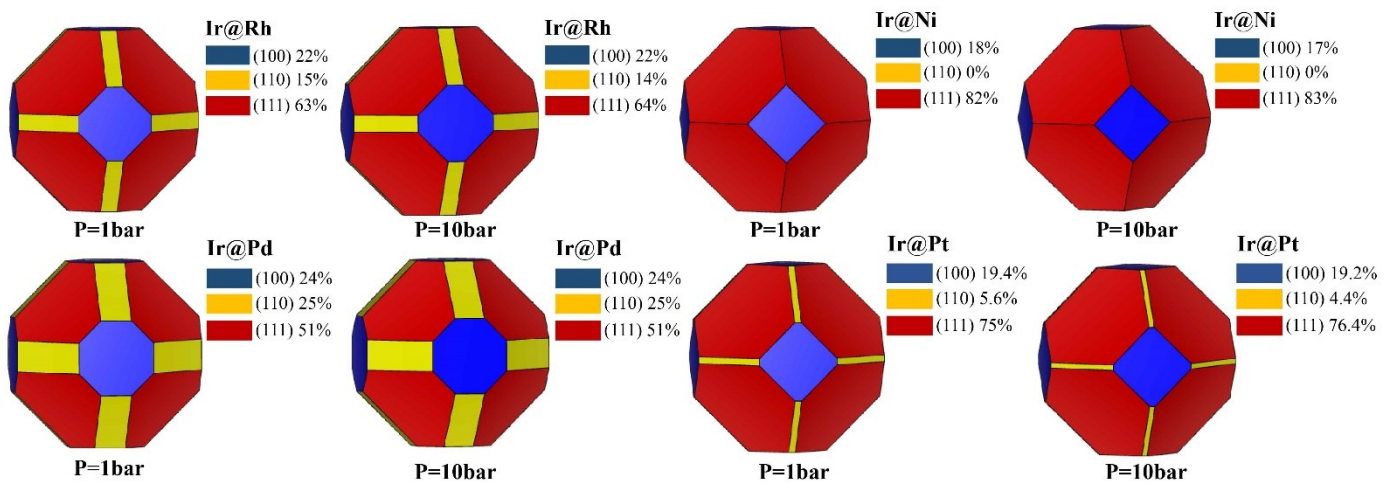


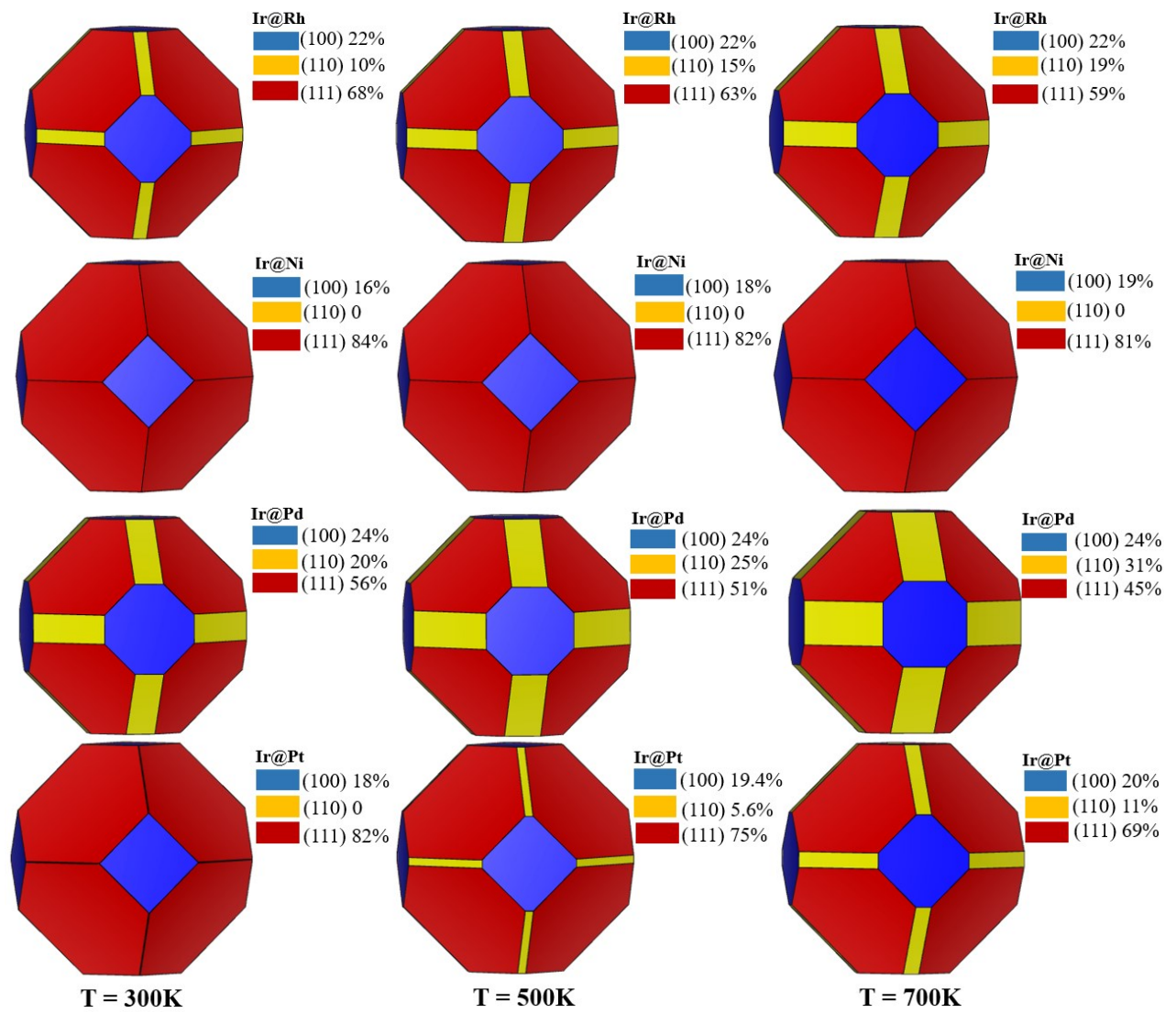
Figure S4: Transition states of methane activation on different alloy metal surfaces including (100), (110) and (111) surfaces.



FigureS5: Wulff structures of Ir@M alloy at different pressures.



FigureS6: Wulff structures of Ir@M alloy at different temperatures.



References:

- [1] W. Lai, D. Xie, D.H. Zhang, First-principles study of adsorption of methyl, coadsorption of methyl and hydrogen, and methane dissociation on Ni(100), *Surface Science*, 594 (2005) 83-92.
- [2] B. Xing, X.-Y. Pang, G.-C. Wang, C-H bond activation of methane on clean and oxygen pre-covered metals: A systematic theoretical study, *Journal of Catalysis*, 282 (2011) 74-82.
- [3] Y.-A. Zhu, Y.-C. Dai, D. Chen, W.-K. Yuan, First-principles calculations of CH₄ dissociation on Ni(100) surface along different reaction pathways, *Journal of Molecular Catalysis A: Chemical*, 264 (2007) 299-308.
- [4] T.H. Upton, Theoretical studies of the decomposition of methanol on Ni(100), *Journal of Vacuum Science and Technology*, 20 (1982) 527-531.
- [5] Steven E. Wonchoba, Donald G. Truhlar, Embedded Diatomics-in-Molecules Potential Energy Function for Methyl Radical and Methane on Nickel Surfaces, *Journal of Physical Chemistry B* 102 (1998) 6842-6860